Topographic and vegetation effects on snow accumulation in the southern Sierra Nevada: a statistical summary from Lidar data

Z. Zheng[1], P. B. Kirchner[2,3], R. C. Bales[1,4]

[1] Department of Civil and Environmental Engineering, UC Berkeley, Berkeley, CA, USA

[2] Joint Institute for Regional Earth System Science and Engineering, Pasadena, CA, USA

[3] Southwest Alaska Network, National Park Service, Anchorage, AK, USA

[4] Sierra Nevada Research Institute, UC Merced, Merced, CA, USA

Correspondence to: Z. Zheng (zeshi.z@berkeley.edu)

Abstract

Airborne light detection and ranging (Lidar) measurements collected in the southern Sierra Nevada near peak snow accumulation in 2010, and in the snow-free season, were analyzed for topographic and vegetation effects on snow accumulation. Combining point-cloud data from four sites separated by 10 to 64 km, with total surveyed area over 106 km^2, it was observed that in the mixed-conifer forest the percent of pixels with snow-depth measurements is sensitive to the sampling resolution used in processing the point cloud. This is apparently due to Lidar not receiving returns from under the denser canopy. The 1-m gridded data show that in addition to elevation effects, snow depth depends strongly on slope, aspect and canopy penetration fraction. A multivariate linear-regression model using all physiographic variables explained 15-25% more variability in snow depth than did a univariate linear-regression model with elevation as a single predictor. However, the weight that each physiographic variable exerted on snow depth varied across different elevation ranges, as well as with different canopy-cover amounts. The difference in mean snow depth in open areas versus under canopy increased with elevation in the rain-snow transition zone (1500-1800 m); and was about 35 ± 10 cm above 1800 m, with the 20-cm fluctuation range reflecting the effects of other topographic variables.

1. Introduction

In the western United States, ecosystem processes and water supplies for agricultural and urban users depend on the mountain snowpack as the primary source of late-spring and early summer streamflow (Bales et al., 2006). Knowledge of spring snowpack conditions within a watershed is essential if water availability and flood peaks following the onset of melt are to be accurately predicted (Hopkinson et al., 2001). California's multi-billion dollar agricultural economy as well as multi-trillion dollar urban economy depend on these predictions (California Department of Water Resources, 2013). Both topographic and vegetation factors are important in influencing the snowpack conditions, as they closely interact with meteorological conditions to affect precipitation and snow distribution in the mountains (McMillen, 1988; Raupach, 1991; Wigmosta et al., 1994). However, mountain precipitation is poorly understood at multiple spatial scales because it is governed by processes that are neither well measured nor accurately predicted (Kirchner et al., 2014). Snow accumulation across the mountains is primarily influenced by orographic processes, involving feedbacks between atmospheric circulation and terrain (Roe, 2005; Roe and Baker, 2006). In most forested regions, snow distribution is highly sensitive to vegetation structure (Anderson, 1963; Revuelto et al., 2015; Musselman et al., 2008); and canopy interception, sublimation as well as unloading result in less accumulation of snow beneath the forest canopies in comparison with canopy gaps (Berris and Harr, 1987; Golding and Swanson, 1986; Mahat and Tarboton, 2013; Sturm, 1992).

The Sierra Nevada is ideally suited for studying mountain snow distribution and related hydrologic processes because it serves as a barrier to moisture moving inland from the Pacific, has an ideal orientation for producing orographic precipitation, and thus exerts a strong influence on the upslope amplification of precipitation (Colle, 2004; Rotach and Zardi, 2007; Smith and

Barstad, 2004). Recent studies provide insight on how orographic and topographic factors affect snow depth in the Alps (Grünewald et al., 2013; Grünewald, et al., 2014; Lehning et al., 2011), suggesting that similar studies could be extended to the Sierra Nevada. And among the forested regions of the mountains, the mixed-conifer and subalpine zones cover most of the high-elevation, seasonally snow-covered area.

In situ, operational measurements of snow water equivalent (SWE) in the Sierra Nevada come from monthly manual snow surveys and daily snow-pillow observations (Rosenberg et al., 2011). Meteorological stations and remote-sensing products also provide estimates of precipitation and snow accumulation (Guan et al., 2013). Cost, data coverage, accuracy (Julander et al., 1998) and basin-scale representativeness are issues for *in situ* monitoring of SWE in mountainous terrain (Rice and Bales, 2010). Satellite-based remote sensing, such as MODIS, has been used to map snow coverage in large or even global areas. However, it only provides snow-coverage information in open areas, and no direct information on snow depths (Molotch and Margulis, 2008). The SNOw Data Assimilation System (SNODAS) integrates data from satellite and *in situ* measurements with weather-forecast and physically based snow models, providing gridded SWE and snow-depth estimates (Barrett, 2003). However, since SNODAS has not been broadly assessed (Clow et al., 2012), its potential for evaluating snow distribution in mountain areas remains uncertain. Also, owing to its 1-km spatial resolution, the snow depth that SNODAS provides is a mixed representation of both open and canopy-covered areas.

An orographic-lift effect is observable in most of the above data (Howat and Tulaczyk, 2005; Rice et al., 2011), and a binary-regression-tree model using topographic variables as predictors has also been used for estimating the snow depth in unmeasured areas (Erickson et al., 2005; Erxleben et al., 2002; Molotch et al., 2005). However, regression coefficients could not be

74 estimated accurately for most of the explanatory variables, except for elevation; and the
75 consistency of the orographic trend as well as the relative importance of these variables is still
76 unknown owing to the lack of representative measurements across different slopes, aspects and
77 canopy conditions. Also, the stability of the variance explained by the model needs to be tested
78 with denser measurements.

79 In recent years, airborne Lidar has been used for high-spatial-resolution distance
80 measurements (Hopkinson et al., 2004), and has become an important technique to acquire
81 topographic data with sub-meter resolution and accuracy (Marks and Bates, 2000). Therefore,
82 Lidar provides a potential tool to help understand spatially distributed snow depth across
83 mountain regions. With multiple returns from a single laser pulse, Lidar has also been used to
84 construct vegetation structures as well as observe conditions under the canopy, which helps
85 produce fine-resolution digital elevation models (DEMs), vegetation structures, and snow-depth
86 information. However, the snow depth under canopy can not always be measured because of the
87 signal-intensity attenuation caused by canopy interception (Deems and Painter, 2006; Deems et
88 al., 2006). A recent report applied a univariate-regression model to the snow depth measured in
89 open areas using Lidar; with a high-resolution DEM used to accurately quantify the orographic-
90 lift effect on the snow accumulation just prior to melt (Kirchner et al., 2014). From this analysis
91 it could be expected that Lidar data might also help explain additional sources of snow
92 distribution variability in complex, forested terrain.

93 The objective of this work reported here is to improve our understanding of how
94 topographic and vegetation factors affect snow accumulation in mixed-conifer forests. We used
95 Lidar data collected in four headwater areas in the southern Sierra Nevada and address the
96 following three questions. First, what new information about orographic effects on precipitation

versus accumulation is provided by these Lidar data? Second, is it possible to have snow-depth measurements in forested mountain terrain from all pixels on a fine sampling resolution (1-5 m) using Lidar data? If not, how does the percentage of pixels measured change with the sampling resolution. Third, what is the importance of slope, aspect and canopy penetration fraction on snow accumulation, relative to elevation; and are effects consistent across sites?

2. Methods

2.1 Study Areas

Our study areas are located in the southern Sierra Nevada, approximately 80 km east of Fresno, California (Figure 1). The four headwater-catchment research areas, Bull Creek, Shorthair Creek, Providence Creek, and Wolverton Basin were previously instrumented, including meteorological measurements, in order to have a better knowledge of the hydrologic processes in this region (Bales et al., 2011; Hunsaker et al., 2012; Kirchner et al., 2014). The sites were chosen as part of multi-disciplinary investigations at the Southern Sierra Critical Zone Observatory, and are also the main instrumented sites in the observatory. Wolverton is approximately 64 km southeast of the other three sites (Figure 1) and is located in Sequoia National Park. Both snow-on and snow-off airborne Lidar were flown in 2010 (Table 1) over these sites. The elevation of the survey areas is from 1600-m to 3500-m elevation. Vegetation density generally decreases in high-elevation subalpine forest, with Wolverton also having a large area above treeline (Goulden et al., 2012). The precipitation has historically been mostly snow in the cold and wet winters for elevations above 2000 m, and a rain-snow mix below 2000 m, where most of Providence is located. The comparison between Providence and the other sites can help in assessing if observed trends are consistent above and below the rain-snow transition.

2.2 Data Collection

All airborne Lidar surveys were performed by the National Center for Airborne Laser Mapping (NCALM) using Optech GEMINI Airborne Laser Terrain Mapper. The scan angle and scan frequency were adjusted to ensure a uniform along-track and across-track point spacing (Table 2), with six GPS ground stations used for determining aircraft trajectory. The snow-on survey date was close to April 1st, which is used by operational agencies as the date of peak snow accumulation for the Sierra. Since the snow-on survey required four days to cover the four study areas, time-series *in situ* snow-depth data measured continuously from Judd Communications ultrasonic depth sensors at Providence, Bull and Wolverton were used to estimate changes in snow depth during the survey period. While no snow accumulation was observed, snowpack densification and melting observed from the time-series data were taken into considerations (Hunsaker et al., 2012; Kirchner et al., 2014). The snow-off survey was performed in August after snow had completely melted out in the study areas.

2.3 Data Processing

Raw Lidar datasets were pre-processed by NCALM and are available from the NSF Open-Topography website (http://opentopography.org) in LAS format. The LAS point cloud, including both canopy and ground-surface points, are stored and classified as ground return and vegetation return. The 1-m resolution digital-elevation models, generated from the Lidar point-cloud datasets, were downloaded from the OpenTopography database and further processed in ArcMap 10.2 to generate 1-m resolution slope, aspect, and northness raster products. Northness is an index for the potential amount of solar radiation reaching a slope on a scale of -1 to 1, calculated from:

$$N = \sin(S) \times \cos(A), \quad (1)$$

where N is the northness value; S is the slope angle and A is the aspect angle, both in degrees. For aspect angle A, north is either 0° or 360°. Northness is also the same as the aspect intensity (Kirchner et al., 2014) with 0° focal aspect. Since in this analysis the snow-depth comparison is only discussed between north and south facing slopes, northness is used instead of aspect intensity for simplification. To construct the 1-m resolution canopy-height models from Lidar data, the 1-m digital-elevation models were subtracted from the 1-m digital-surface models that rasterized from the first return of the laser pulses (Figure 2).

The snow depths were calculated directly from the snow-on Lidar data. By referring to canopy-height models, all ground points in snow-on Lidar datasets were classified as under canopy or in open areas. That is, if the ground point was coincident with canopy of >2-m height, it was classified as under canopy, and otherwise in the open, i.e., a 2-m height was used to classify shrubs versus trees. In this study we assumed the shrubs did not affect the snow depth. After classification, snow depths were calculated by subtracting the values in the digital-elevation model from the snow-on point-measurement values. The calculated point snow-depth data were further assigned into 1-m raster pixels, averaged within each pixel, formatted and then gap filled by interpolation with pixel values around it. Since not all laser pulses that generated canopy-surface returns had ground returns (Figure 3) and the ground-return percentage varied across the transition from the tree trunk to the edge of the canopy, interpolation was not applied to data under the canopy. The error rate of the calculated snow depth should be mainly from the instrumental elevation error, which is about 0.10 m (Kirchner et al., 2014; Nolan et al., 2015).

2.4 Penetration Fraction

The open-canopy fraction is a factor that represents the forest density above a given pixel and is used to describe the influence of vegetation on snow accumulation and melt. However there is no algorithm to directly extract this information from Lidar data. Here we use a novel approach we call penetration fraction to approximate the open-canopy fraction from the Lidar point cloud, with which we were able to quantify the impact of canopy on snow depth using linear regression. Penetration fraction is the ratio of the number of ground points to number of total points within each pixel (Figure 4a). Whereas pixels are generally classified as under canopy or in the open (Kirchner et al., 2014), penetration fraction is an index of fraction open in a pixel. Because the electromagnetic radiation from both Lidar and sunlight beams are intercepted by canopies, the open-canopy fraction is used here as an index to represent the fraction of sunlight radiance received on the ground under vegetation. Therefore, penetration fraction of Lidar is actually another form of estimating the open-canopy fraction (Musselman et al., 2013). However, under-canopy vegetation can also intercept the Lidar beam, causing a bias. To eliminate this bias, the canopy-height model was used to check if the pixel was canopy covered by using the 2-m threshold value; and if not, the local penetration fraction of the pixel was reset to 1 because the open-canopy fraction of a pixel could not be entirely represented by the penetration fraction. A spatial moving-average process was applied using a 2-D Gaussian filter to account for the effect of the vegetation around each pixel. Since the radius of the Gaussian filter needs to be specified by the user, we tested the sensitivity of smoothing results to the radius of the filter and found it is not sensitive when the radius is greater than 1.5 m (Figure 4b). Therefore, we specified a radius of 5 m in the Gaussian filter.

2.5 Statistical Analysis

The 1-m resolution snow-depth raster datasets were resampled into 2-m, 3-m, 4-m and 5-m resolution. The percentage of pixels with snow-depth measurements was calculated by using the number of pixels with valid data divided by the total number of pixels inside each site. The sensitivity of the percentage changes across different resampling resolutions and the consistency of the percentages across study sites at the same resampling resolution were analyzed by visualizing the percentages against sampling resolutions at all sites.

Using elevation, slope, aspect, penetration fraction and snow depth retrieved from Lidar measurements, topographic and vegetation effects on snow accumulation were observed using residual analysis. Owing to orographic effects, there is increasing precipitation along an increasing elevation gradient in this area (Kirchner et al., 2014). Therefore, elevation was selected as the primary variable to fit the linear-regression model for calculating the residual of snow depth. All snow-depth measurements from Lidar were first separated by either under canopy or in open areas, and then were binned by elevation of the location where they were measured, with a bin size of 1-m elevation. As each elevation band had hundreds of snow-depth measurements after binning, the average of all snow depths was chosen as the representative snow depth, and the standard deviation calculated to represent the snow-depth variability within each elevation band. Coefficients of determination between snow depth and elevation of each site were calculated by linear regression. The fitted linear-regression model of each site was applied to the DEM to estimate the snow depth. The residual of snow depth was calculated by subtracting the modeled snow depth from Lidar-measured snow depth. The slope, aspect and penetration fraction were binned into 1° slope, 1° aspect, and 1% penetration-fraction bins with snow-depth residuals corresponding to each bin of every physiographic variable averaged and visualized along the variable gradient to check the existence of these physiographic effects.

For the variables found to correlate with the snow accumulation, the relative importance of each variable was calculated using the Random Forest algorithm (Breiman, 2001; Pedregosa and Varoquaux, 2011). A multivariate linear-regression model was also fitted to all physiographic variables to calculate the regression coefficients, which could be used as the effect of that variable on the snow distribution.

To calculate the snow-depth difference between open and canopy-covered area along an elevation gradient, the 1-m resolution snow-depth data of the two conditions, open and canopy-covered, were smoothed separately against elevation using locally weighted scatterplot smoothing (LOESS) (Cleveland, 1979). The snow-depth difference was then calculated by subtracting the smoothed canopy-covered snow depth from that in open.

3. Results

The percentage of pixels having snow-depth measurements is highly sensitive to the sampling resolution used in processing the Lidar point cloud to produce the raster data. The percentage goes from about 65 to 90% across the 4 sites for 1-m resolution and gradually increases to 100% at 5-m resolution (Figure 5). Note that the percentage increases in going from the lower to higher elevation sites, consistent with lower forest density decreasing at higher elevation.

The snow depth in open areas and under canopy show consistent increasing trends with elevation across all sites (Figure 6a, 6b). Although orographic effects may vary between individual storms across sites, these data suggest that the effect of the 4 main snowfall events prior to the Lidar data collection date (Kirchner, 2013) resulted in similar patterns. The variability within an elevation band for open area (Figure 6c) is highest at about 1500 m, and gradually decreases within the rain-snow transition up to 2000-m elevation. However, at above

2000 m, the pattern of variability with increasing elevation varies across sites. Note that values at the upper or lower ends of elevation at each site have few pixels and maybe less representative of the value of physiographic attributes in the study areas (Figure 6d). The forested area, of all four sites combined, spans the rain-snow transition zone in mixed conifer through subalpine forest to significant areas above treeline.

For each individual site, a least-squares linear regression of averaged snow depth versus elevation was used to investigate the spatial variability of snow depth (Table 3). The median elevation of the three sites increases from Providence to Bull to Shorthair. The lowest elevation at Providence Creek is less than 1400 m, and snow depth increases steeply in this region at a rate of 38 cm per 100 m in open areas and 28 cm per 100 m under the canopy. Bull Creek has an elevation range of 2000-2400 meters, which is slightly higher than Providence, and has snow depth increasing at 21 cm per 100 m in open areas and 19 cm per 100 m under the canopy. For Shorthair Creek site, which is the highest of the three, the snow depth increases at 17 cm per 100 m in open areas and 16 cm per 100 m under the canopy. Wolverton is 64 km further south and spans a wider elevation range, going from the rain-snow transition in mixed conifer, to subalpine forest, to some area above treeline. The average snow-depth increase is smallest among all four study sites, 15 cm per 100 m in open areas and 13 cm per 100 m under the canopy. Unlike the other three lower-elevation sites, the snow depth at Wolverton site decreases above 3300-m elevation and these high-elevation data were not modeled with the linear regression. The amount of area above this elevation is relatively small, and factors such as wind redistribution and the exhaustion of perceptible water can also affect snow depth at these elevations (Kirchner et al., 2014).

255 The residuals for the snow in the open areas were further analyzed for effects of slope,
256 aspect and penetration fraction. The snow-depth residual increases negatively about 10 to 40 cm
257 as slope angle increases from 0° to 60°; and the residual changes from positive 0-50 cm to
258 negative 20-60 cm in going from north-facing to south-facing slopes (Figure 7a, 7b). The
259 topographic effect can also be seen from the color pattern of northness observed in the
260 scatterplots (Figure 5a, 5b). The residual also changes from negative 20-40 cm to positive 20-40
261 cm as penetration fraction increases from 0% to 80% (Figure 7c). Considering all of these
262 variables together, elevation is the most important variable at all sites except for Shorthair, which
263 has a relatively small elevation range (Figure 8). Aspect exerts a stronger influence than do slope
264 and penetration fraction in open areas. However, for under-canopy areas, penetration is more
265 dominant than aspect at two sites. The multivariate regression model was fitted to the data with
266 aspect transformed into 0° to 180° range (north to south). Fitted models can be represented as
267 the following two equations for open area and under canopy respectively:

268 $$SD = 0.0011 \times Elevation - 0.0112 \times Slope - 0.0057 \times Aspect + 0.1802 \times Penetration \quad (2)$$

269 $$SD = 0.0009 \times Elevation - 0.0128 \times Slope - 0.0046 \times Aspect + 0.9891 \times Penetration \quad (3)$$

270 where SD is snow depth and p-values of all regression coefficients of the two models are all
271 smaller than 0.01. The effects quantified in these two equations are mixtures of influences that
272 exerted during both precipitation processes and post-deposition processes.

273 The snow-depth difference between open and canopy-covered area was calculated with
274 elevation from locally smoothed snow depth (Figure 9). It generally increases from near zero at
275 1500 m, where there is little snow but dense canopy, to 40 cm in the range of 1800-2000 m, and
276 varies from near zero to 60 cm at higher elevations where snow is deeper and the canopy less
277 dense. It is apparent that the snow-depth difference increases with elevation in the rain-snow

transition zone, but lacks a clean pattern along either elevation gradient or penetration-fraction gradient when the elevation is higher.

4. Discussion

4.1 Sensitivity of measurements to sampling resolution

The results of the percentage of pixels with snow depth measured from Lidar data at different sampling resolutions illustrate that even high-density airborne Lidar measurements do not have 100% coverage of the surveyed area at 1-m resolution, especially in densely forested areas. According to the snow-depth difference between snowpack in open areas and under canopy, the trade-off between accuracy and coverage happens when adjusting the resolution; and lower sampling resolutions can introduce overestimation into the results. This is because upon averaging, sub-pixel area under the canopy that was not measured is represented by the open that is measured, introducing an overestimation error into the averaged snow depth of the pixel. In order to estimate that bias for each pixel, we would need more under-canopy snow-depth measurements at 1-m resolution. In our survey areas, 10-35% of the total areas need to be densely measured. Besides, an average overestimation bias could be estimated over the main snow-producing elevation range of 2000-3000 m. Since using open rather than under-canopy values would introduce a bias of about 35 cm over 20-35% of the area, a 2-m mean snow depth in 2000-3000 m elevation will have about 10 cm or 5% overestimation. Therefore, the sampling resolution for processing the Lidar point cloud needs to be chosen according to the objective and accuracy tolerance of the study and the average overestimation bias needs to be corrected for the study results.

4.2 Physiographic effect on snow accumulation

Below 3300 m, the increasing trend of snow accumulation with elevation was observed for all sites (Figure 6). Linear regression is applicable to model the relationship between snow depth and elevation when the study area has a broad elevation range. This holds true for all of our sites with the exception of Shorthair, where the elevation range is about 200 m and the coefficient of determination for this linear-regression model is much smaller than the other three sites, which have ranges greater than 500 m. The bias of mean snow depth in the same elevation band between different sites is acceptable if the standard error is added or subtracted from the mean (Figure 6a, 6b, 6c). The data-collection time, spatial variation and variations of other topographic features should introduce bias across sites. However, as data-collection time only differs a few days, *in situ* snow-depth sensor data suggest that the melting and densification effect was under 2 cm (https://czo.ucmerced.edu/dataCatalog_sierra.html). As for other topographic variables, the observation of a slope effect, shown as the trend lines in Figure 7a and the negative regression coefficients of the two linear-regression models, could be explained by steeper slopes having higher avalanche potential, fewer trees and thus more wind; and thus some snow is more likely to be lost from these slopes. Snowpack located in south-facing slopes receives higher solar radiation, with the snowmelt being accelerated (Kirchner et al., 2014). This explains the trends observed in Figure 7b and the negative regression coefficients of the multivariate models. Although Lidar has measurement errors caused by slope and aspect (Baltsavias, 1999; Deems et al., 2013; Hodgson and Bresnahan, 2004), error is not able to be quantified and traced back to each variable and we assumed its influence on the trends could be neglected. As canopy interception results in reduced snow depth under canopy, the snow-depth residuals are found changing from negative to positive with penetration fraction and the regression coefficients are positive (Figure 7c). The multivariate linear-regression model built

from the Lidar data is a significant improvement, as the variability of the snow distribution could explain 15-25% more than the univariate linear-regression model with elevation as the only predictive variable (Table 4) and the estimation bias has a narrower distribution (Figure 10a, 10b). Also, fitting an individual linear-regression model for each site is slightly better than using a general model with all sites' data involved (Figure 10c, 10d) and it might because that an individual model could capture regional micro-climate within the site better than a general model. The opposite trend of the relative importance of predictive variables observed in Shorthair is because it is a relatively flat site (Figure 1, Figure 8), which implies that topographic variables other than elevation need to be focused more when studying about areas with small elevation ranges in future works.

4.3 Vegetation effects on snow distribution along elevation

Under-canopy snow distribution is governed by multiple factors that affect the energy environment, as observed by melting (Essery et al., 2008; Gelfan et al., 2004) and accumulation rates (Pomeroy et al., 1998; Schmidt and Gluns, 1991; Teti, 2003). Our results show different responses when comparing the snow-depth difference between open and canopy-covered areas between study sites (Figure 9a). In the rain-snow transition zone from 1500 to 2000 m of Providence we see a sharp linear increase between open and under-canopy snow depth that is likely governed by the under-canopy energy environment and the canopy-interception effect on precipitation, which accelerate snowmelt and prevent accumulation of under-canopy snow. Above 2000 m, the snow-depth difference observed at Bull and Shorthair stabilized around 40 cm and 20 cm respectively, with fluctuations less than 10 cm along elevation. Breaking from this pattern, the large dip in snow-depth difference, down to 10 cm, observed at Wolverton at elevations of 2250-2750 m deviates from the 35-40 cm plateau. Also, the snow-depth difference

346 at Shorthair stabilizes around 20 cm, which is 20 cm lower than the stabilized value at Bull.
347 Based on the scatterplot in Figure 6a and 6b that color coded by northness, at elevation range of
348 2300-2700 m, there are a lot more data points with both low snow depth and extremely negative
349 northness in the open area than under the canopy, which implies that anisotropic distribution of
350 other topographic variables is affecting the snow-depth difference. This is further shown by
351 filtering out the data points not within a small certain range (-0.1 to 0.1) of northness, and then
352 reproducing Figure 9a using the filtered data. As presented in Figure 11, it is apparent that the
353 large dip at Wolverton is flattened out to a canopy effect of around 25-45 cm as the topographic
354 effect is filtered out. Thus a sigmoidal function was used to characterize the snow-depth
355 difference changes with elevation excluding topographic interactions. The interactions between
356 topographic variables and vegetation is most likely attributable to the under-canopy snowpack
357 being less sensitive to solar radiation versus snowpack in the open area (Courbaud et al., 2003;
358 Dubayah, 1994; Essery et al., 2008; Musselman et al., 2008, 2012).

359 In spite of filtering the topographic effect, there is still about a 20-cm magnitude of
360 fluctuation in the snow-depth difference, which might be attributed to various clearing sizes of
361 open area at different locations and various vegetation types in the forests (Hedstrom and
362 Pomeroy, 1998; Pomeroy et al., 2002; Schmidt and Gluns, 1991), however, these features of the
363 sites are not able to be explored from this Lidar dataset.

364 ## 5. Conclusions

365 As an advanced and promising remote-sensing technology, Lidar is able to measure snow
366 depth of 100% survey area at 5-m sampling resolution however the accuracy is still left to be
367 evaluated because of lacking enough representative measurements under the canopy. A 1-m

368 resolution processed Lidar dataset is more accurate but the percentage of pixels with
369 measurements is much less than 100%.

370 Using processed Lidar data sampled at 1-m resolution, averaged snow depth within each
371 1-m elevation band shows a strong correlation with elevation at all sites, indicating that snow
372 accumulation in the southern Sierra Nevada is primarily affected by orographic lift. Snow-depth
373 residuals calculated by de-trending the elevation dependency are correlated with slope, aspect
374 and penetration fraction, which shows the effect of additional physiographic variables on snow
375 accumulation other than elevation. The relative importance of these variables in predicting snow
376 depth implies that other than elevation, aspect affects snow-accumulation and retention more in
377 open areas, while penetration fraction is as important as aspect for snow under the canopy. More
378 significantly, a multivariate linear-regression model fitted with variables for slope, aspect and
379 canopy penetration fraction explains 15-25% more snow-depth variability than using elevation as
380 the only predictive variable, suggesting multiple predictive variables will be more effective for
381 quantifying the water equivalent in the Sierra Nevada at peak snow accumulation.

382 The snow-depth difference between open and canopy-covered areas increases in the rain-
383 snow transition elevation range and then stabilized around 25-45 cm at high elevation. Large
384 magnitude of fluctuations are presented at certain elevation ranges in Wolverton and Shorthair,
385 which is partially due to interactions from other topographic variables, evidence of which is
386 found by filtering the northness into a narrow band and which causes the fluctuations flattening
387 out.

Acknowledgements. This material is based on data and processing services provided by the OpenTopograhy Facility with support from the National Science Foundation under NSF Award Numbers 1226353 & 1225810. Research was supported by the National Science Foundation under NSF Award Numbers 1331939 & 1239521 and UC Water Security and Sustainability Research Initiative funded by the University of California Office of the President (UCOP) (Grant No. 13941). We acknowledge the helpful comments from Q. Guo, A. Harpold, and N.P. Molotch, also Q. Guo and J. Flanagan for providing canopy height model data.

Reference

Anderson, H. W.: Managing California's Snow Zone Lands for Water, Pacific Southwest For. Range Exp. Station. Berkeley, CA, 34, 1963.

Bales, R. C., Molotch, N. P., Painter, T. H., Dettinger, M. D., Rice, R. and Dozier, J.: Mountain hydrology of the western United States, Water Resour. Res., 42(8), n/a–n/a, doi:10.1029/2005WR004387, 2006.

Bales, R. C., Hopmans, J. W., O'Geen, A. T., Meadows, M., Hartsough, P. C., Kirchner, P., Hunsaker, C. T. and Beaudette, D.: Soil Moisture Response to Snowmelt and Rainfall in a Sierra Nevada Mixed-Conifer Forest, Vadose Zo. J., 10(3), 786, doi:10.2136/vzj2011.0001, 2011.

Baltsavias, E.: Airborne laser scanning: basic relations and formulas, ISPRS J. Photogramm. Remote Sens., (54), 199–214 [online] Available from: http://www2.geog.ucl.ac.uk/~mdisney/teaching/teachingNEW/PPRS/papers/Baltsavias_Lidar.pdf, 1999.

Barrett, A. P.: National Operational Hydrologic Remote Sensing Center SNOw Data Assimilation System (SNODAS) Products at NSIDC, NSIDC Spec. Rep. 11, (Natl. Snow and Ice Data Cent.: Boulder, CO), 19, 2003.

Berris, S. N. and Harr, R. D.: Comparative snow accumulation and melt during rainfall in forested and clear-cut plots in the Western Cascades of Oregon, Water Resour. Res., 23(1), 135, doi:10.1029/WR023i001p00135, 1987.

Breiman, L. (University of C.: Random forest, Mach. Learn., 45(1), 5–32, doi:10.1023/A:1010933404324, 2001.

California Department of Water Resources: California ' s Flood Future : Recommendations for Managing the State ' s Flood Risk., 2013.

Cleveland, W. S.: Robust Locally Weighted Regression and Smoothing Scatterplots, J. Am. Stat. Assoc., 74(368), 829–836, doi:10.2307/2286407, 1979.

Clow, D. W., Nanus, L., Verdin, K. L. and Schmidt, J.: Evaluation of SNODAS snow depth and snow water equivalent estimates for the Colorado Rocky Mountains, USA, Hydrol. Process., 26(17), 2583–2591, doi:10.1002/hyp.9385, 2012.

Colle, B. a.: Sensitivity of Orographic Precipitation to Changing Ambient Conditions and Terrain Geometries: An Idealized Modeling Perspective, J. Atmos. Sci., 61(5), 588–606, doi:10.1175/1520-0469(2004)061<0588:SOOPTC>2.0.CO;2, 2004.

Courbaud, B., De Coligny, F. and Cordonnier, T.: Simulating radiation distribution in a

428 heterogeneous Norway spruce forest on a slope, Agric. For. Meteorol., 116(1-2), 1–18,
429 doi:10.1016/S0168-1923(02)00254-X, 2003.

430 Deems, J. S. and Painter, T. H.: Lidar measurement of snow depth: accuracy and error
431 sources, Proc. 2006 Int. Snow Sci. Work. Telluride, Color. USA, Int. Snow Sci. Work., 330,
432 330–338, 2006.

433 Deems, J. S., Fassnacht, S. R. and Elder, K. J.: Fractal Distribution of Snow Depth from Lidar
434 Data, J. Hydrometeorol., 7(2), 285–297, 2006.

435 Deems, J. S., Painter, T. H. and Finnegan, D. C.: Lidar measurement of snow depth: a review, J.
436 Glaciol., 59(215), 467–479, doi:10.3189/2013JoG12J154, 2013.

437 Dubayah, R. C.: Modeling a solar radiation topoclimatology for the Rio Grande River Basin, J.
438 Veg. Sci., 5(5), 627–640, doi:10.2307/3235879, 1994.

439 Erickson, T. a., Williams, M. W. and Winstral, A.: Persistence of topographic controls on the
440 spatial distribution of snow in rugged mountain terrain, Colorado, United States, Water
441 Resour. Res., 41(4), 1–17, doi:10.1029/2003WR002973, 2005.

442 Erxleben, J., Elder, K. and Davis, R.: Comparison of spatial interpolation methods for
443 estimating snow distribution in the Colorado Rocky Mountains, Hydrol. Process., 16(18),
444 3627–3649, doi:10.1002/hyp.1239, 2002.

445 Essery, R., Bunting, P., Rowlands, A., Rutter, N., Hardy, J., Melloh, R., Link, T., Marks, D. and
446 Pomeroy, J.: Radiative Transfer Modeling of a Coniferous Canopy Characterized by
447 Airborne Remote Sensing, J. Hydrometeorol., 9(2), 228–241, doi:10.1175/2007JHM870.1,
448 2008.

449 Gelfan, a. N., Pomeroy, J. W. and Kuchment, L. S.: Modeling Forest Cover Influences on Snow
450 Accumulation, Sublimation, and Melt, J. Hydrometeorol., 5(5), 785–803, doi:10.1175/1525-
451 7541(2004)005<0785:MFCIOS>2.0.CO;2, 2004.

452 Golding, D. L. and Swanson, R. H.: Snow distribution patterns in clearings and adjacent
453 forest, Water Resour. Res., 22(13), 1931, doi:10.1029/WR022i013p01931, 1986.

454 Goulden, M. L., Anderson, R. G., Bales, R. C., Kelly, a. E., Meadows, M. and Winston, G. C.:
455 Evapotranspiration along an elevation gradient in California's Sierra Nevada, J. Geophys.
456 Res. Biogeosciences, 117(3), 1–13, doi:10.1029/2012JG002027, 2012.

457 Grünewald, T., Stötter, J., Pomeroy, J. W., Dadic, R., Moreno Baños, I., Marturià, J., Spross, M.,
458 Hopkinson, C., Burlando, P. and Lehning, M.: Statistical modelling of the snow depth
459 distribution in open alpine terrain, Hydrol. Earth Syst. Sci., 17(8), 3005–3021,
460 doi:10.5194/hess-17-3005-2013, 2013.

461 Grünewald, T., Bühler, Y. and Lehning, M.: Elevation dependency of mountain snow depth,
462 Cryosph., 8(6), 2381–2394, doi:10.5194/tc-8-2381-2014, 2014.

463 Guan, B., Molotch, N. P., Waliser, D. E., Jepsen, S. M., Painter, T. H. and Dozier, J.: Snow water
464 equivalent in the Sierra Nevada: Blending snow sensor observations with snowmelt model
465 simulations, Water Resour. Res., 49(8), 5029–5046, doi:10.1002/wrcr.20387, 2013.

466 Hedstrom, N. R. and Pomeroy, J. W.: Measurements and modelling of snow interception in
467 the boreal forest, Hydrol. Process., 12(10-11), 1611–1625, doi:10.1002/(SICI)1099-
468 1085(199808/09)12:10/11<1611::AID-HYP684>3.0.CO;2-4, 1998.

469 Hodgson, M. E. and Bresnahan, P.: Accuracy of Airborne Lidar-Derived Elevation : Empirical
470 Assessment and Error Budget, Photogramm. Eng. Remote Sensing, 70(3), 331–339, 2004.

471 Hopkinson, C., Sitar, M., Chasmer, L., Gynan, C., Agro, D., Enter, R., Foster, J., Heels, N.,
472 Hoffman, C., Nillson, J. and Others: Mapping the spatial distribution of snowpack depth
473 beneath a variable forest canopy using airborne laser altimetry, Proc. 58th Annu. East.
474 Snow Conf., 2001.

475 Hopkinson, C., Sitar, M., Chasmer, L. and Treitz, P.: Mapping snowpack depth beneath forest
476 canopies using airborne lidar., Photogramm. Eng. Remote Sens., 70(3), 323–330, 2004.

477 Howat, I. M. and Tulaczyk, S.: Trends in spring snowpack over a half-century of climate
478 warming in California, USA, Ann. Glaciol., 40, 151–156, doi:10.3189/172756405781813816,
479 2005.

480 Hunsaker, C. T., Whitaker, T. W. and Bales, R. C.: Snowmelt Runoff and Water Yield Along
481 Elevation and Temperature Gradients in California's Southern Sierra Nevada1, JAWRA J.
482 Am. Water Resour. Assoc., 48(4), 667–678, doi:10.1111/j.1752-1688.2012.00641.x, 2012.

483 J. Revuelto, J. I. Lo?pez-Moreno, C. A.-M. and Vicente-Serrano, S. M.: Canopy influence on
484 snow depth distribution in a pine stand determined from terrestrial laser data, Water
485 Resour. Res., doi:10.1002/2014WR016496, 2015.

486 Kirchner, P. B.: Dissertation for the degree of Doctor of Philosophy, University of California,
487 Merced., 2013.

488 Kirchner, P. B., Bales, R. C., Molotch, N. P., Flanagan, J. and Guo, Q.: LiDAR measurement of
489 seasonal snow accumulation along an elevation gradient in the southern Sierra Nevada,
490 California, Hydrol. Earth Syst. Sci. Discuss., 11, 5327–5365, doi:10.5194/hessd-11-5327-
491 2014, 2014.

492 Lehning, M., Grünewald, T. and Schirmer, M.: Mountain snow distribution governed by an
493 altitudinal gradient and terrain roughness, Geophys. Res. Lett., 38(19), 1–5,

494 doi:10.1029/2011GL048927, 2011.

495 Mahat, V. and Tarboton, D. G.: Representation of canopy snow interception, unloading and
496 melt in a parsimonious snowmelt model, Hydrol. Process., 6336(December 2013), n/a–n/a,
497 doi:10.1002/hyp.10116, 2013.

498 Marks, K. and Bates, P.: Integration of high-resolution topographic data with floodplain
499 flow models, Hydrol. Process., 14(July 1998), 2109–2122, doi:10.1002/1099-
500 1085(20000815/30)14:11/12<2109::AID-HYP58>3.0.CO;2-1, 2000.

501 McMillen, R. T.: An eddy correlation technique with extended applicability to non-simple
502 terrain, Boundary-Layer Meteorol., 43(3), 231–245, doi:10.1007/BF00128405, 1988.

503 Molotch, N. P. and Margulis, S. a.: Estimating the distribution of snow water equivalent
504 using remotely sensed snow cover data and a spatially distributed snowmelt model: A
505 multi-resolution, multi-sensor comparison, Adv. Water Resour., 31(11), 1503–1514,
506 doi:10.1016/j.advwatres.2008.07.017, 2008.

507 Molotch, N. P., Colee, M. T., Bales, R. C. and Dozier, J.: Estimating the spatial distribution of
508 snow water equivalent in an alpine basin using binary regression tree models: The impact
509 of digital elevation data and independent variable selection, Hydrol. Process., 19(December
510 2004), 1459–1479, doi:10.1002/hyp.5586, 2005.

511 Musselman, K. N., Molotch, N. P. and Brooks, P. D.: Effects of vegetation on snow
512 accumulation and ablation in a mid-latitude sub-alpine forest, Hydrol. Process., 22(15),
513 2767–2776, doi:10.1002/hyp, 2008.

514 Musselman, K. N., Molotch, N. P., Margulis, S. a., Kirchner, P. B. and Bales, R. C.: Influence of
515 canopy structure and direct beam solar irradiance on snowmelt rates in a mixed conifer
516 forest, Agric. For. Meteorol., 161, 46–56, doi:10.1016/j.agrformet.2012.03.011, 2012.

517 Musselman, K. N., Margulis, S. a. and Molotch, N. P.: Estimation of solar direct beam
518 transmittance of conifer canopies from airborne LiDAR, Remote Sens. Environ., 136, 402–
519 415, doi:10.1016/j.rse.2013.05.021, 2013.

520 Nolan, M., Larsen, C. and Sturm, M.: Mapping snow-depth from manned-aircraft on
521 landscape scales at centimeter resolution using Structure-from-Motion photogrammetry,
522 Cryosph. Discuss., 9, 333–381, doi:10.5194/tcd-9-333-2015, 2015.

523 Pedregosa, F. and Varoquaux, G.: Scikit-learn: Machine Learning in Python, J. Mach. ..., 12,
524 2825–2830 [online] Available from:
525 http://jmlr.csail.mit.edu/papers/volume12/pedregosa11a/pedregosa11a.pdf, 2011.

526 Pomeroy, J. W., Parviainen, J., Hedstrom, N. and Gray, D. M.: Coupled modelling of forest

527 snow interception and sublimation, Hydrol. Process., 12(15), 2317–2337,
528 doi:10.1002/(SICI)1099-1085(199812)12:15<2317::AID-HYP799>3.0.CO;2-X, 1998.

529 Pomeroy, J. W., Gray, D. M., Hedstrom, N. R. and Janowicz, J. R.: Prediction of seasonal snow
530 accumulation in cold climate forests, Hydrol. Process., 16(18), 3543–3558,
531 doi:10.1002/hyp.1228, 2002.

532 Raupach, M. R.: Vegetation-atmosphere interaction in homogeneous and heterogeneous
533 terrain: some implications of mixed-layer dynamics, Vegetatio, 91(1-2), 105–120,
534 doi:10.1007/BF00036051, 1991.

535 Rice, R. and Bales, R. C.: Embedded-sensor network design for snow cover measurements
536 around snow pillow and snow course sites in the Sierra Nevada of California, Water Resour.
537 Res., 46(3), 1–13, doi:10.1029/2008WR007318, 2010.

538 Rice, R., Bales, R. C., Painter, T. H. and Dozier, J.: Snow water equivalent along elevation
539 gradients in the Merced and Tuolumne River basins of the Sierra Nevada, Water Resour.
540 Res., 47(8), n/a–n/a, doi:10.1029/2010WR009278, 2011.

541 Roe, G. H.: Orographic Precipitation, Annu. Rev. Earth Planet. Sci., 33(1), 645–671,
542 doi:10.1146/annurev.earth.33.092203.122541, 2005.

543 Roe, G. H. and Baker, M. B.: Microphysical and Geometrical Controls on the Pattern of
544 Orographic Precipitation, J. Atmos. Sci., 63(3), 861–880, doi:10.1175/JAS3619.1, 2006.

545 Rosenberg, E. a., Wood, A. W. and Steinemann, A. C.: Statistical applications of physically
546 based hydrologic models to seasonal streamflow forecasts, Water Resour. Res., 47(3), n/a–
547 n/a, doi:10.1029/2010WR010101, 2011.

548 Rotach, M. W. and Zardi, D.: On the boundary-layer structure over highly complex terrain:
549 Key findings from MAP, Q. J. R. …, 133, 937–948, doi:10.1002/qj, 2007.

550 Schmidt, R. a. and Gluns, D. R.: Snowfall interception on branches of three conifer species,
551 Can. J. For. Res., doi:10.1139/x91-176, 1991.

552 Smith, R. B. and Barstad, I.: A Linear Theory of Orographic Precipitation, J. Atmos. Sci.,
553 61(12), 1377–1391, doi:10.1175/1520-0469(2004)061<1377:ALTOOP>2.0.CO;2, 2004.

554 Sturm, M.: Snow distribution and heat flow in the taiga, Arctic, Antarct. Alp. Res., 24(2),
555 145–152, 1992.

556 Teti, P.: Relations between peak snow accumulation and canopy density, For. Chron., 79(2),
557 307–312, 2003.

558 Wigmosta, M. S., Vail, L. W. and Lettenmaier, D. P.: A distributed hydrology-vegetation
559 model for complex terrain, Water Resour. Res., 30(6), 1665–1680,

560 doi:10.1029/94WR00436, 1994.

561

1 Table 1. Lidar data collection information

	Bull	Shorthair	Providence	Wolverton
Snow-off flight date	August 15, 2010	August 13, 2010	August 5, 2010	August 13-15, 2010
Snow-on flight date	March 24, 2010	March 23, 2010	March 23, 2010	March 21-22, 2010
Area, km^2	22.3	6.8	18.4	58.9
Mean elevation, m	2264	2651	1850	2840
Elevation range, m	1925-2490	2436-2754	1373-2207	1786-3523
Canopy cover, %	50.3	43.4	63.2	38.6

2

3 Table 2. Flight parameters and sensor settings

Flight parameters		Equipment settings	
flight altitude	600 m	wavelength	1047 nm
flight speed	65 m s^{-1}	beam divergence	0.25 mrad
swath width	233.26 m	laser PRF	100 kHz
Swath overlap	50%	scan frequency	55 Hz
point density	10.27 p m^{-2}	scan angle	±14°
Cross track res	0.233 m	scan cutoff	3°
Down track res	0.418 m	scan offset	0°

4 Table 3. Linear regression of averaged snow depth vs. elevation in four sites

	Bull	Shorthair	Providence	Wolverton
Open R^2	0.968	0.797	0.931	0.914
Vegetated R^2	0.978	0.737	0.921	0.972
Open slope, cm per 100 m	21.6	16.1	37.8	15.3
Vegetated slope, cm per 100 m	19.9	13.1	26.0	13.4

5 Table 4. Coefficients of determination of univariate and multivariate linear-regression models

	Univariate model R^2	Multivariate model R^2
Bull	0.23	0.37
Shorthair	0.06	0.32
Providence	0.39	0.53
Wolverton	0.16	0.38
All sites	0.43	0.57

6

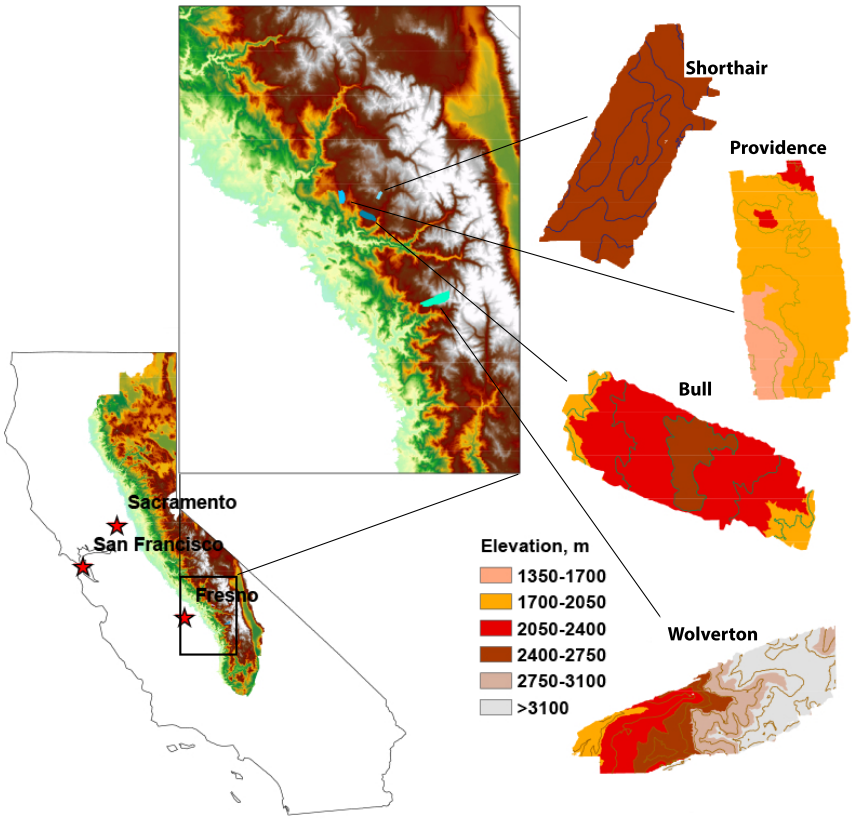

Figure 1. Study area and Lidar footprints. (Left) California with Sierra Nevada. (Center) Zoomed view to show the locations of Lidar footprints. (Right) Elevation and 200-m contour map (100-m for Bull) of Lidar footprints

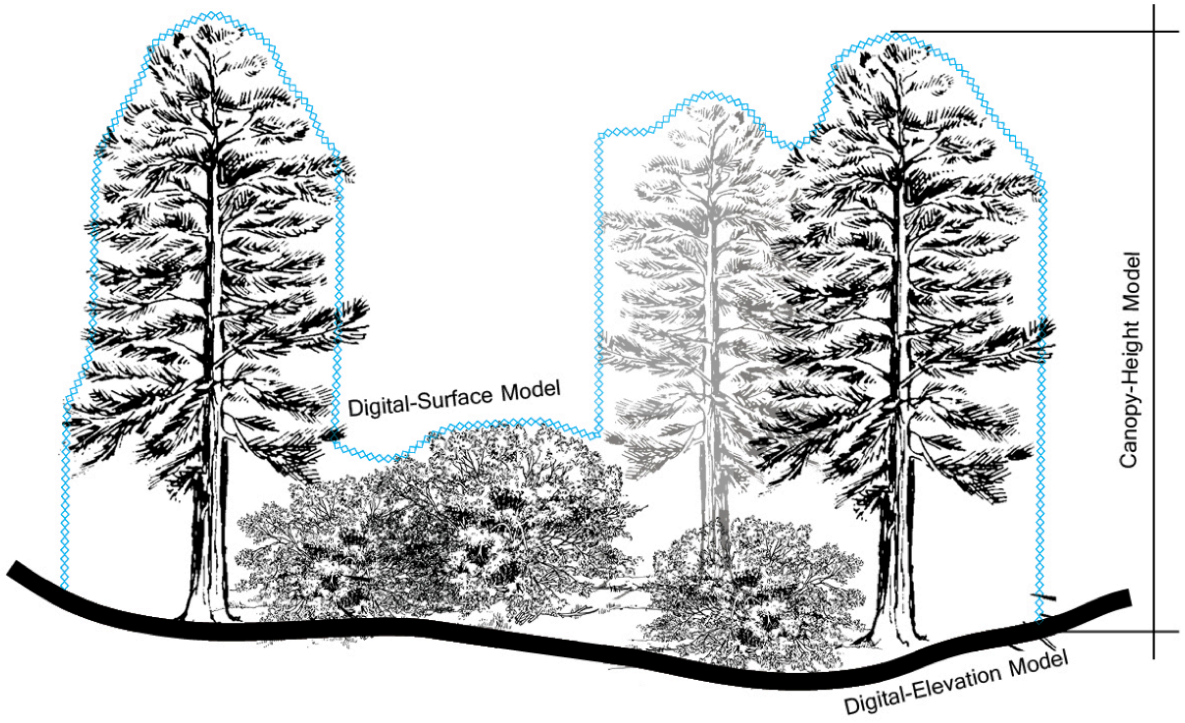

Figure 2. Subtracting the digital-elevation model from the digital-surface model will result in the canopy-height model. In this study the height of shrub vegetation is assumed smaller than 2 m while tree vegetation is taller than 2 m.

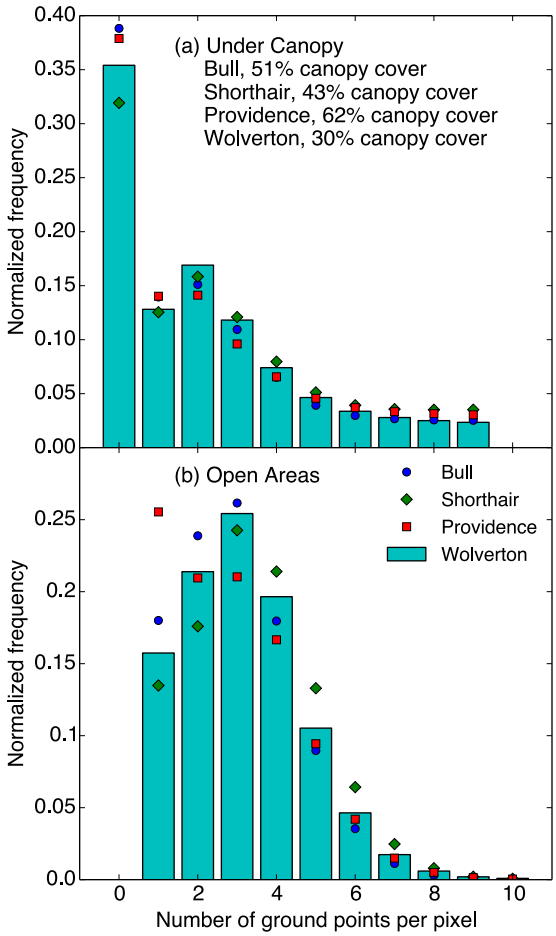

Figure 3. (a) Normalized histogram of the number of ground points for under canopy pixels. (b) Normalized histogram of the number of ground points in open pixels.

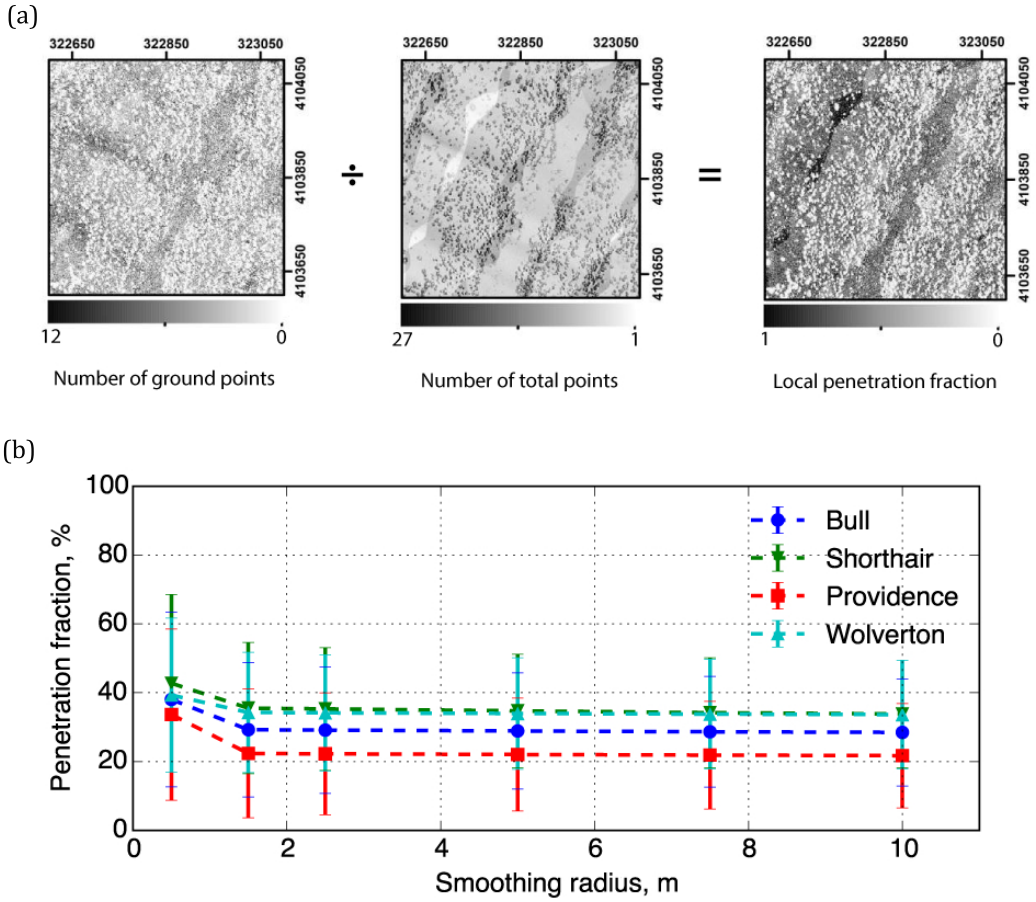

Figure 4. (a) Dividing the number of ground points of each 1-m pixel by the total number of points in the pixel will result the penetration fraction of the local pixel. (b) Sensitivity of the smoothed penetration fraction to the smoothing radius, showing that the result is not sensitivity as the radius is larger than 1.5 m.

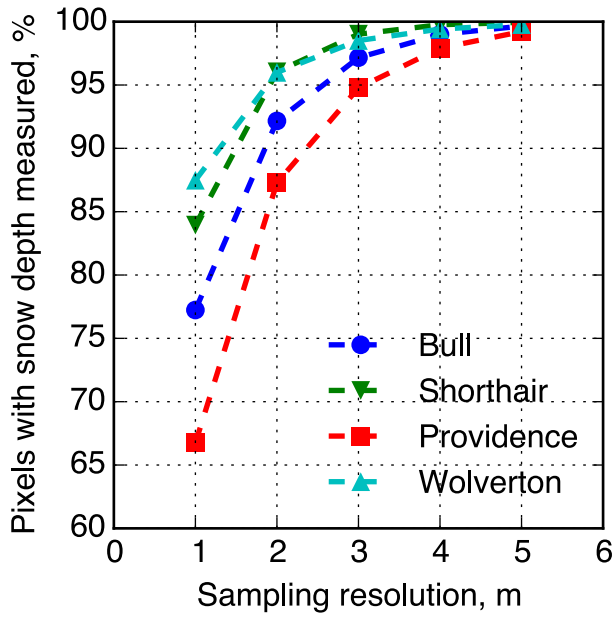

Figure 5. Sensitivity of the percentage of pixels with snow depth measured to the sampling resolution used in processing the Lidar point cloud at each site.

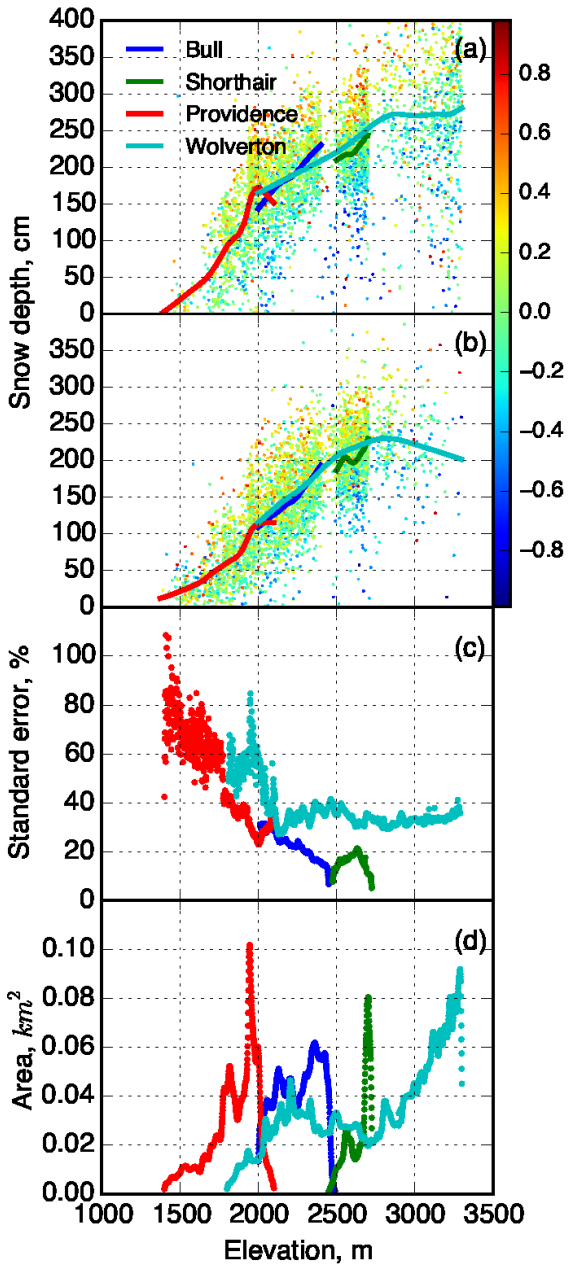

25

26 Figure 6. LOESS smoothed snow depth with northness color coded scatterplot of raw-pixel snow depth
27 against elevation for (a) open area (b) under-canopy area. (c) Standard error of the snow depth within
28 each 1-m elevation band for open area. (d) Total area of each elevation band for both open and under-
29 canopy area. Values above 3300 m not shown, where there are few data.

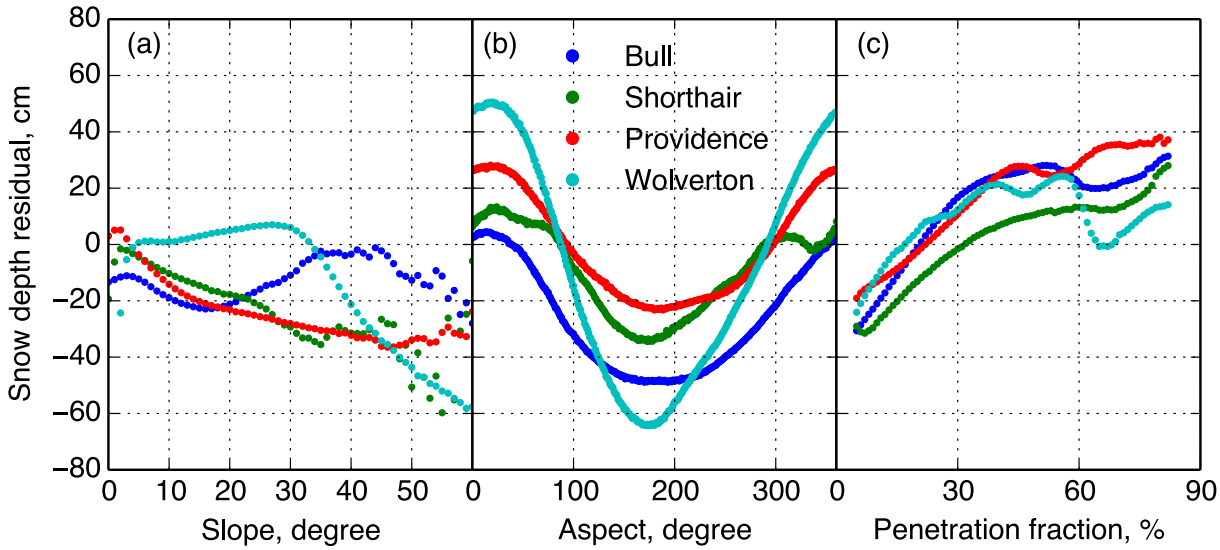

Figure 7. (a) Averaged snow-depth residual along slope. Raw snow-depth residual was calculated from Lidar measured snow depth and estimated snow depth from the linear-regression models (open areas). (b) Averaged snow-depth residual along aspect. (c) Averaged snow-depth residual along penetration fraction.

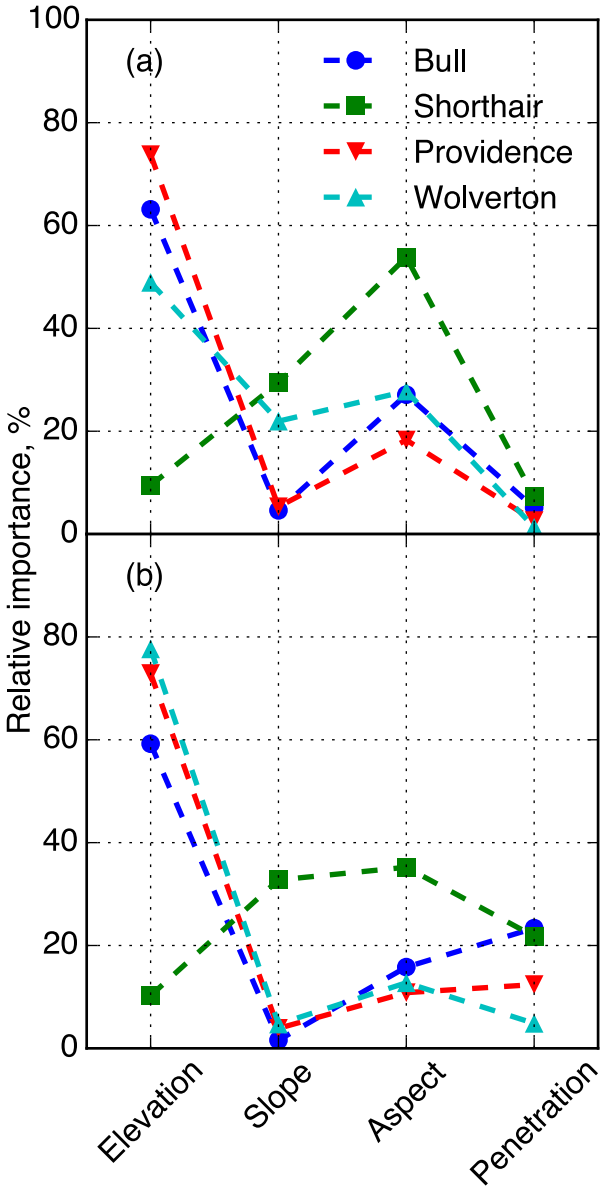

Figure 8. Relative importance of each physiographic variable in predicting the snow depth from each site for (a) open area (b) under-canopy area

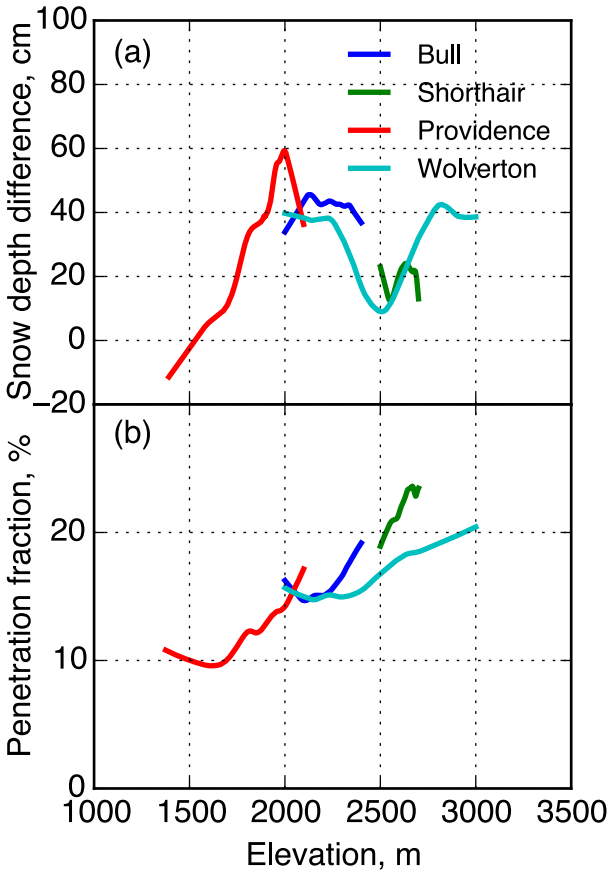

Figure 9. (a) Snow-depth difference along elevation for each site calculated from the LOESS smoothed snow depth. (b) Averaged penetration fraction along elevation gradient for each site.

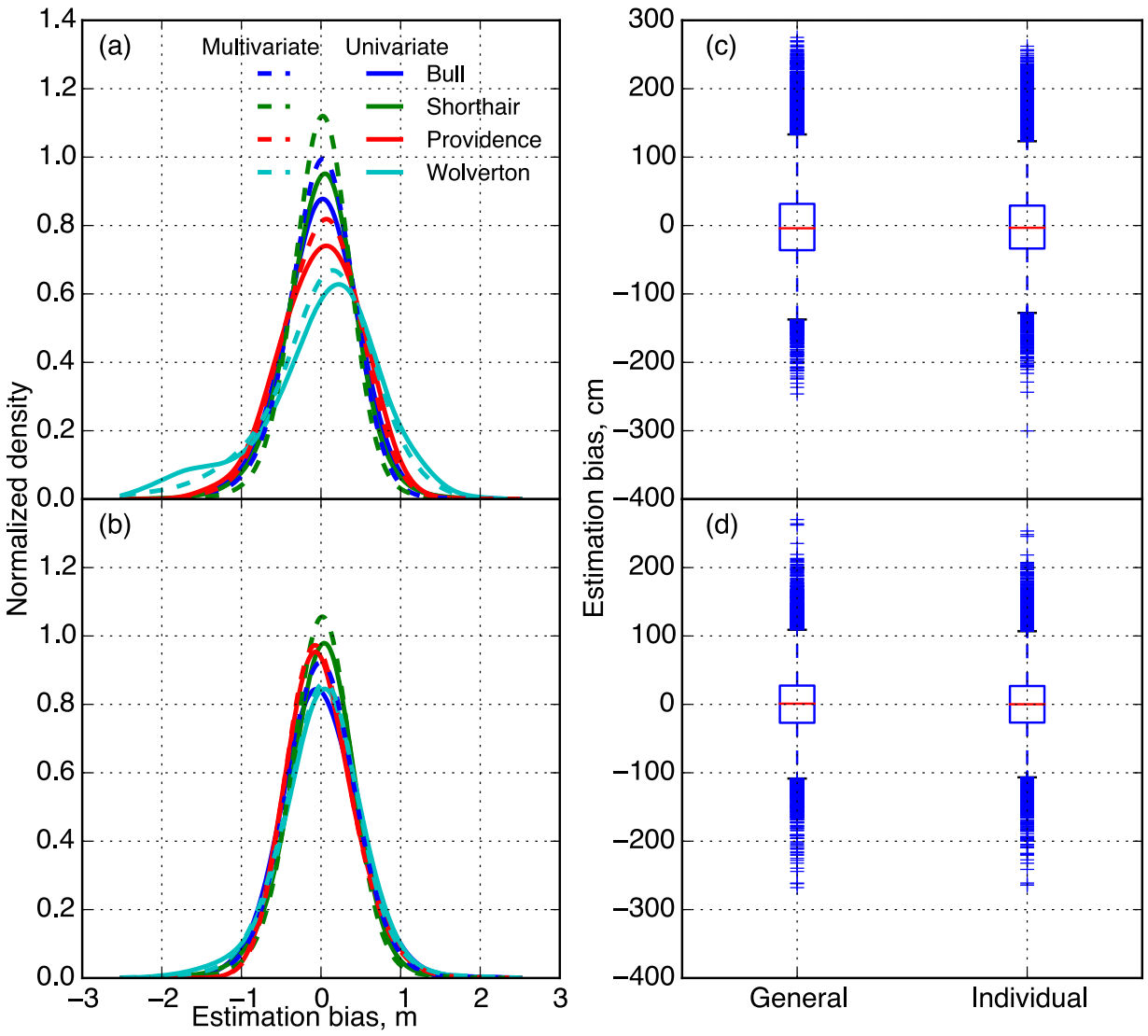

40

41 Figure 10. Normalized density of estimation bias for (a) open area (b) under-canopy area; Estimation bias
42 boxplots of using one general linear-regression model with all sites' data combined and four linear-
43 regression models of each individual site for (c) open area (d) under-canopy area.

44

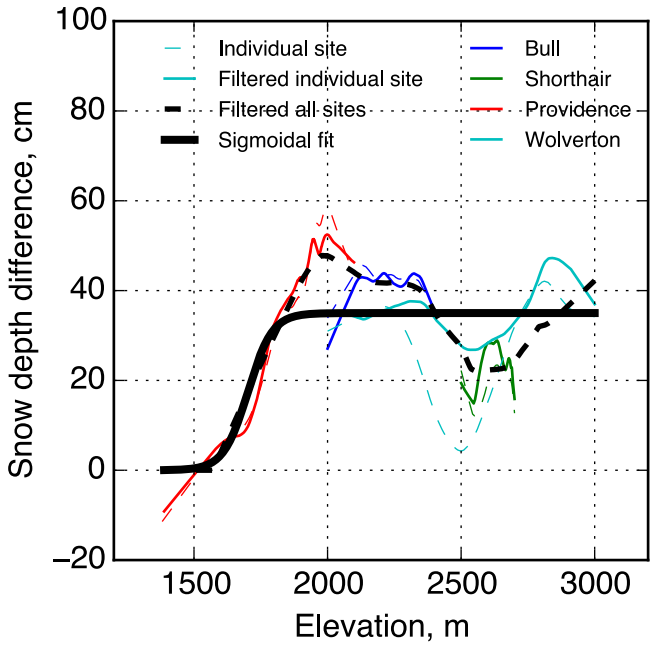

45

46 Figure 11. Snow-depth difference between open and under-canopy area: comparison between
47 using raw 1-m pixel snow depth and northness-filtered 1-m pixel snow depth, together with the
48 sigmoidal fit of the snow-depth difference changing with elevation

49